

CELL-SELECTIVE PROTEOMICS OF METHICILLIN-RESISTANT
STAPHYLOCOCCUS AUREUS (MRSA) INFECTION IN MICE
IDENTIFIES A NOVEL ANTI-VIRULENCE TARGET

3.1 Abstract

Methicillin-resistant *Staphylococcus aureus* (MRSA) poses a threat to human health and is becoming increasingly resistant to current antibiotics. Characterizing the MRSA proteome during an infection *in vivo* would reveal important information about the process of infection and potentially reveal new strategies to fight the disease. Currently available proteomic techniques, however, are not capable of efficiently measuring pathogen proteins among the highly abundant host protein background that is inherent to infection models. In this work we use bioorthogonal noncanonical amino acid tagging (BONCAT) to perform cell-selective proteomic analysis of MRSA in a mouse skin infection model, identifying 766 MRSA proteins synthesized during infection. Quantitative analysis of our dataset identifies novel virulence factors that are upregulated during the course of infection. Deletion of AdhE, one of the top BONCAT hit proteins, led to a significant decrease in MRSA virulence phenotype during infection. Furthermore, a point mutation within AdhE reduced virulence to levels similar to that of the full deletion, indicating a novel site for targeted anti-virulence therapies. Overall, this work demonstrates the importance of cell-selective chemoproteomic labeling *in vivo* and provides insight into the pathogenesis of MRSA infections, revealing several promising targets for anti-virulence therapy development.

This work was a collaborative effort with Arya Khosravi, Brett M. Babin, Michael J. Sweredoski, John D. Bagert, Will H. DePas, Annie Moradian, Alborz Mahdavi, Hwan Kim, Fabiana Falugi, Sonja Hess, Dianne K. Newman, Olaf Schneewind, Dominique Missiakas, and Sarkis K. Mazmanian.

Significance Statement

This work uses a novel chemoproteomic method to tag and detect newly synthesized proteins by a pathogen in a mouse model of skin infection. By specifically incorporating a label into proteins synthesized by methicillin-resistant *Staphylococcus aureus* (MRSA) as it infects its mouse host, proteins important for nutrient acquisition, metabolism, and pathogenesis were identified. We tested whether these proteins contributed to infection by assaying strains of MRSA with single deletions in them. One deletion demonstrated a significant decrease in infection, indicating that this protein contributes to MRSA pathogenesis and could be a novel target for antibiotics. Overall, our findings underscore the ability of bioorthogonal noncanonical amino acid tagging (BONCAT) to “fish out” pathogenic proteins from more abundant host ones, suggesting that this strategy could be used for other infectious pathogens.

3.2 Introduction

Methicillin-resistant *Staphylococcus aureus* (MRSA), a pathogen that causes life-threatening infections, poses a serious human health threat due to the increasing numbers of multidrug resistant strains and a lack of new antibiotics (1, 2). Anti-infective drugs, which target bacteria during invasion, have been suggested as alternative or adjunct therapies to antibiotics, as they increase bacterial susceptibility (3). By targeting factors uniquely expressed *in vivo*, such antibiotics would not affect bacteria growing outside the host, thus decreasing the possibility of evolved resistance (4). A catalog of virulence factors uniquely expressed during infection is required for continual efforts to

develop anti-infective agents. Elucidating the *in vivo* staphylococcal proteome during infection, however, is challenging due to the technical limitations of shotgun proteomics: the relative overabundance of host proteins occupy most of a mass spectrometer's bandwidth, which strongly represses the detection of proteins from the pathogen. Previous studies have attempted to overcome this limitation by enriching for bacteria using cell sorting. These approaches, however, are prone to artifacts during sample preparation, are blind to secreted proteins, and are not amenable to certain biological systems (5, 6). Other studies attempt to mimic the nutrient status of the host in test tubes, but do not fully recapitulate the complex environment of the host (7, 8).

Bioorthogonal noncanonical amino acid tagging (BONCAT) is a chemoproteomic technique that enables the cell-selective and temporal labeling of the cellular proteome (9). With this technique, a mutant aminoacyl-tRNA synthetase expressed solely by the cells of interest allows for selective incorporation of a noncanonical amino acid (ncAA) with a bioorthogonal handle into proteins for subsequent detection and identification. Because cellular proteins are only labeled during the ncAA pulse, BONCAT provides a temporally precise overview of the cell's proteome. The chemical handles on the ncAAs, often azides or alkynes, can then be conjugated to fluorophores or enrichment tags using copper-catalyzed alkyne-azide cycloaddition (CuAAC) or strain-promoted alkyne-azide cycloaddition (SPAAC) (10, 11). Notably, all of these reagents including the ncAAs are commercially available. BONCAT has previously been applied to studies of microbial pathogenesis in *in vitro* models of infection (11-15). Herein, we adapted BONCAT to a

mouse model of skin infection and identified the proteome of MRSA *in vivo* (Fig 3.1).

Our findings highlight the ability of BONCAT to selectively enrich for pathogenic proteins from the highly abundant host protein background in the complex milieu of an active skin infection. Labeling is pathogen-specific and can be achieved within 4 hours and subsequently used to enrich for staphylococcal proteins made within a host. Testing potential candidates from this list for virulence defects *in vivo* led to the discovery of a novel protein important for MRSA infection. We expect that this unbiased approach to label pathogenic proteins could be used as a global discovery tool for novel anti-infective strategies since it is compatible with other pathogens and modes of infection, and uses commercially available reagents.

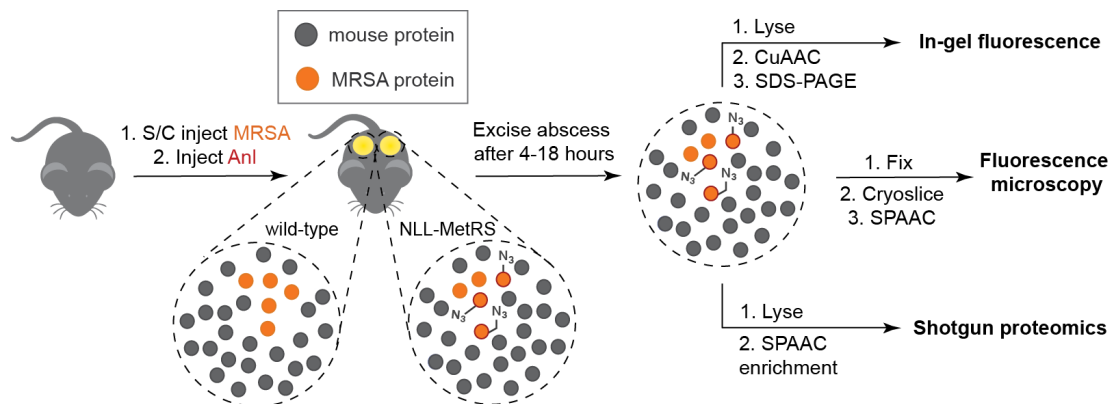


Figure 3.1: Schematic depicting BONCAT to label MRSA in a mouse model of skin infection. Strains of MRSA that do not express NLL-MetRS are unable to incorporate azidonorleucine (Anl) into proteins. Azide-labeled proteins are subsequently visualized using fluorescence microscopy or enriched for proteomic detection.

3.3 Results

Adapting cell-selective BONCAT for MRSA. We first needed to adapt cell-selective BONCAT for use in MRSA. We opted to use a mutant methionyl-tRNA synthetase (NLL-MetRS) previously employed in studies of host-pathogen interactions that allows for the incorporation of azidonorleucine (Anl) in place of methionine residues (16). The *Escherichia coli* (*Ec*) NLL-MetRS codon-optimized for *Staphylococcus aureus* was inserted into a staphylococcal shuttle plasmid under control of the hprK/lgt promoter, which has been shown to be constitutively active, including during infections *in vivo* (17-19). This plasmid (+NLL) was transformed into the virulent MRSA strain USA300, which accounts for up to 98% of reported skin and soft tissue infections (SSTIs) in hospitals (1). A plasmid without the inserted NLL-MetRS (-NLL) was used as an empty-vector control for all characterizations.

To assess the ability of the *Ec* NLL-MetRS to charge MRSA tRNAs with azidonorleucine (Anl), +NLL and -NLL cultures were grown in tryptic soy broth (TSB) and 2 mM of Anl was added for 1 hour during exponential growth. Protein lysate from treated cells was first conjugated to alkyne-functionalized tetramethylrhodamine (alkyne-TAMRA, Fig S3.1) using CuAAC and then separated by SDS-PAGE for subsequent in-gel fluorescence scanning (Fig S3.2A). Gels revealed selective labeling in the +NLL samples only, signifying that the *Ec* NLL-MetRS had successfully charged Anl onto tRNAs and labeled newly-synthesized proteins within MRSA. Nonspecific incorporation of Anl into the proteome of -NLL strains was not detected. Importantly,

growth did not appear to be affected, even with long (12 hour) pulses of Anl (Fig S3.2B).

Characterizing cell-selective BONCAT labeling during skin infection in a mouse.

The +NLL/-NLL strains of MRSA were then used in a mouse model of early skin infection (4). Following subcutaneous (S/C) injection of the +NLL or -NLL strains along with 25 μ L of 25 mM Anl, we excised and homogenized entire abscesses after 4, 12, and 16 hours of labeling. Conjugation to alkyne-TAMRA followed by in-gel fluorescence revealed Anl labeling at every time point for +NLL MRSA with the strongest labeling occurring 12 to 16 hours post infection (Fig 3.2B, Fig S3.3). As the mouse and the -NLL strain do not express the mutant aminoacyl-tRNA synthetase, Anl is unable to be incorporated into their proteins. Importantly, the size of the lesion formed and the number of colony-forming units (CFUs) obtained from each lesion did not depend on the strain used or on the presence of Anl, suggesting that BONCAT does not perturb the progress of infection (Fig 3.2B).

Visualization of newly synthesized MRSA proteins within skin abscesses. To ensure that Anl labeling was confined to MRSA, we infected with +NLL or -NLL strains of MRSA and subcutaneously injected Anl at the time of infection. After waiting 16 hours to allow for incorporation of Anl into newly synthesized proteins, we excised and cryosectioned whole skin abscesses. We detected Anl labeling by conjugation via SPAAC to aza-dibenzocyclooctyne functionalized with AlexaFluor488 (DBCO-AF488,

Fig S3.1) and immunostained for MRSA proteins using a polyclonal anti-*S. aureus* antibody. We observed DBCO-AF488 staining of proteins in the abscess only when the NLL-MetRS was expressed within MRSA and that this staining co-localized with the anti-*S. aureus* counterstain, suggesting that MRSA protein synthesis could be cell-selectively visualized within the abscesses (Fig 3.2D, Fig S3.4).

Enrichment of Anl-labeled proteins results in greater proteomic coverage of MRSA proteins synthesized *in vivo*. To identify MRSA proteins within the skin abscesses, we labeled proteins in triplicate during the first 16 hours of subcutaneous infection, excised the abscesses, and homogenized the entire abscess. After cell lysis, we enriched for azide-labeled proteins using aza-dibenzocyclooctyne-conjugated agarose beads (DBCO-agarose). A portion of the sample was reserved to serve as an “unenriched” control for comparison. Enriched and unenriched samples were digested with trypsin and subjected to liquid chromatography-tandem mass spectrometry (LC-MS/MS) analysis.

Prior to enrichment, the LC-MS/MS runs were overwhelmed with highly abundant mouse proteins, masking the signal from nearly all MRSA proteins. For example, of all the spectra detected in the unenriched samples, only 3% were assigned to MRSA proteins, and the remaining were attributed to mouse proteins and common contaminants. This finding led to the identification of only 178 MRSA proteins in the unenriched samples.

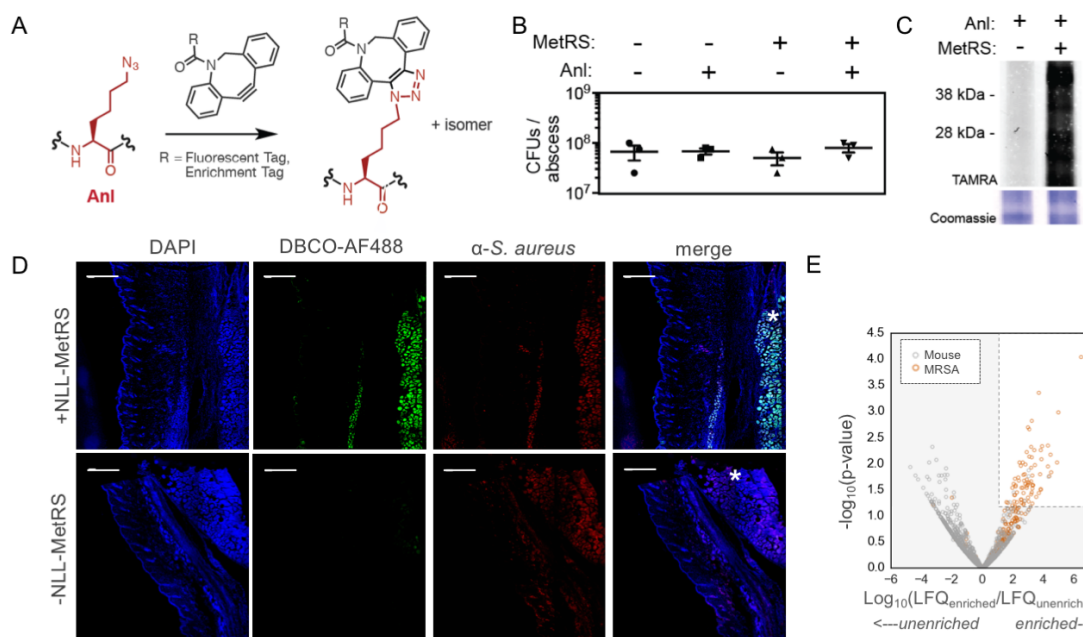


Figure 3.2: BONCAT specifically labels newly synthesized MRSA proteins within skin abscesses. A) Strain-promoted alkyne-azide cycloaddition (SPAAC) for visualization or enrichment of *in vivo* synthesized proteins. B) BONCAT does not affect growth of MRSA *in vivo*. C) Copper-catalyzed alkyne-azide cycloaddition (CuAAC) with TAMRA-alkyne followed by SDS-PAGE enables in-gel fluorescence of labeled proteins. D) Skin infected with +NLL or -NLL MRSA and labeled with Anl for 18 hours. After the abscessed was excised and cryogenically sliced, the samples were blocked, and then reacted to DBCO-AF488, followed by an anti-*S. aureus* antibody. *Indicate abscess. Scale bar is 100 μm . E) Volcano plot of proteins found in both unenriched samples and enriched samples shows that MRSA proteins (orange) are enriched compared to mouse proteins (blue). Most MRSA proteins were uniquely found in enriched samples and do not have fold-change values to exhibit.

With enrichment, 23% of all spectra could be assigned to MRSA proteins, leading to the identification of 766 proteins with at least 1 peptide, which is the largest number of identified MRSA proteins in an *in vivo* infection model to date (Fig S3.5). Additionally,

the identified proteins had greater average intensities, leading to more confident identifications (IDs) and quantifications (Fig S3.5C, S3.5D). Linear Models for Microarray Data (LIMMA), an empirical Bayes (eBayes) method, was then employed to detect significant changes in protein abundances for proteins found before and after enrichment (20, 21). MRSA proteins were significantly more abundant in the enriched samples (Fig 3.2E). Thus, labeling with AnI followed by enrichment increases the number of identified MRSA proteins.

Identifying MRSA proteins important for infection using comparative proteomics.

We sought to identify proteins that are expressed exclusively or highly upregulated within the skin and may serve as promising anti-infective targets. We therefore compared the detected MRSA proteins during skin infection to those made during aerobic and anaerobic growth. The +NLL MRSA strain was grown aerobically in triplicate and labeled with AnI for 1 hour during mid-log growth, then lysed and enriched for proteins synthesized during this time. The same experiment was performed using anaerobic cultures, except for being labeled for 2 hours during mid-log growth. Using this strategy, we quantified 655 proteins expressed during skin infection (at least 2 peptides/protein), 925 proteins expressed during aerobic growth, and 1,055 proteins expressed during anaerobic growth (Fig 3.3A, Table S3.4). The 530 proteins detected in all three environments were then compared using LIMMA and confirmed that NLL-MetRS was expressed at similar levels between the replicates (Fig S3.6A), highlighting the constitutive nature of the chosen promoter.

To determine if the proteins found upregulated in the skin were associated with virulence, we used Gene Ontology (GO) analysis. The log-fold changes of the proteins identified during the skin infection were compared to either aerobically or anaerobically grown cells, and a Mann-Whitney U test was performed to determine if the median values for proteins with the given annotation tended to be higher or lower than those without the annotation. Compared to aerobically and anaerobically grown samples, three GO terms were significantly enriched in both: “cellular catabolic process”, “pathogenesis”, and “small molecule catabolic process” (Fig 3.3B). After plotting the log-fold changes in the skin compared to anaerobic vs. aerobic, proteins annotated with the GO term “pathogenesis” were generally located in the upper right quadrant (Fig 3.3C). The only protein not found in this quadrant, yet annotated as important to pathogenesis, was enolase (Eno), a glycolytic pathway enzyme reported to bind laminin during infection (22). Catabolic processes have been established as important in skin and soft tissue infections due to their low abundance of glucose (23).

Compared to *in vitro* growth, we found many known virulence factors and contributors to infection to be upregulated in our *in vivo* skin infection model (Fig 3B). For example, virulence factors gamma-hemolysin (Hlg), staphylococcal superantigen-like protein 7 (Ssl7), and immunoglobulin-binding protein (Sbi) were uniquely detected during infection (18). Immunoglobulin-binding protein A (Spa) was significantly upregulated *in vivo* compared to aerobic and anaerobic growth conditions. Additionally, staphylococcal accessory regulator SarA and catalase (KatA) were upregulated *in vivo* compared to

anaerobic growth (Fig 3.3C, S3.7-8) (24).

In addition to these known virulence factors, many genes involved in nutrient scavenging were identified using BONCAT. Five of the genes involved in iron acquisition from heme (IsdA, IsdB, IsdC, IsdG, and IsdI) were upregulated during infection (Fig 3.3D, Fig S3.9), which are important due to low iron availability within the mammalian host (25). Proteins upregulated in the arginine catabolic mobile element (ACME: ArcC2 and ArcB) that are important to withstand the acidic environment of the skin (26), and in the endogenous arginine catabolic pathway (ArgF and ArcC1) that degrade arginine under anaerobic conditions (Fig 3.3D, Fig S3.10), were also detected. Additionally, two proteins involved in catabolizing N-acetylneuraminate, the predominant sialic acid in humans (sialic acid lyase (NanA) and NanR), were found only in the skin (Fig 3.4A, Table S3.4).

S. aureus requires distinct sets of proteins for successful infection of different tissues, whereas few genes are required for the pathogenesis of all types of *S. aureus* infections, suggesting a limitation of why several reported virulence genes were not detected using BONCAT (27). Additionally, certain proteins may be too low abundance, not contain any methionine residues besides the initiator, or not ionize well on the mass spectrometer. For example, accessory gene regulator A (AgrA), fibronectin binding protein A (FnbA), nuclease (Nuc), phenol-soluble modulins (PsmA1, PsmA4: which do not contain any methionine residues besides the initiator Met) (28), and the *S. aureus*

exoprotein expression two-component system SaeRS were not detected in the *in vivo* samples.

Because levels of oxygen vary widely within different tissues in the host (17), we wondered whether our infection model more closely resembled aerobically or anaerobically grown samples. We therefore performed a principal component analysis (PCA) on the proteins found in all samples; the replicates clustered in three separate subspaces (Fig 3.3E, Fig S3.16). Based on the proteomic profile, the *in vivo* environment is a distinct growth setting compared to *in vitro* conditions. Performing PCA on the proteins found in aerobically and anaerobically grown samples revealed a single component that accounted for 71% of the variance between the data sets. A projection of the data from the skin infection replicates into this dimension formed a distinct group (Fig S3.5D).

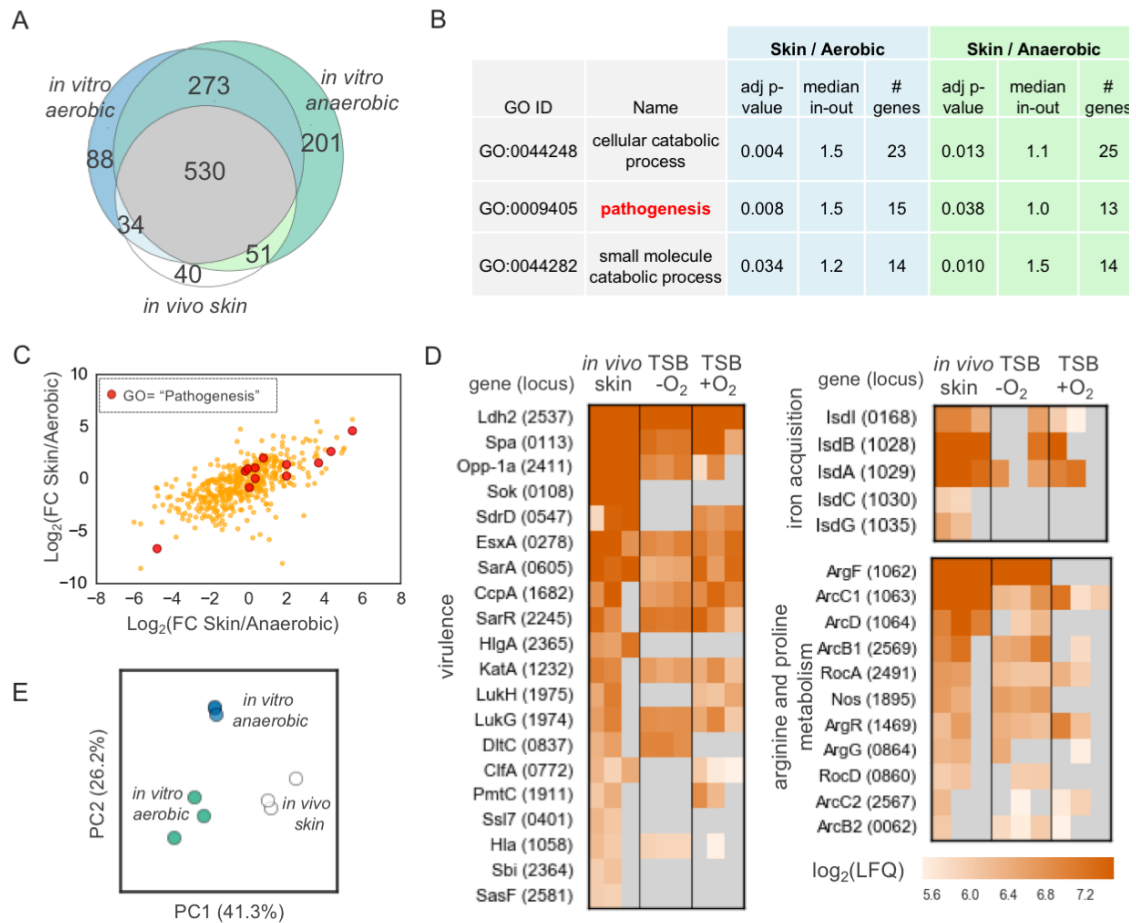


Figure 3.3: Comparative proteomics reveals MRSA proteins expressed during infection. A) Venn diagram of proteins quantified during aerobic or anaerobic growth *in vitro* or during skin infection *in vivo*. B) Gene Ontology (GO) analysis of upregulated pathways during skin infection revealed the terms “catabolic process” and “pathogenesis”. C) Proteins annotated with the GO term “pathogenesis” (red circles) are upregulated compared to aerobic or anaerobic growth. D) Heat maps of proteins annotated to be important to virulence, iron acquisition, or arginine catabolism during all three conditions. E) Principal component analysis (PCA) of proteins found in all samples.

Screening hits from BONCAT analysis reveals AdhE as a novel factor that contributes to virulence. From the list of proteins found upregulated or unique to infection (Table S3.4), 10 proteins that had not been previously associated with infection (Fig 3.4A) (6, 29) were selected. Isogenic knockout mutants of each of these strains, along with known virulence factor sortase ($\Delta srtA$) (2, 22, 25-27), were then used for subsequent studies. SrtA is a target for novel anti-infective therapies due to its ability to display 20 different adhesins on the cell-surface (25, 30). To ascertain if each protein singularly contributed to skin infection, we infected mice using the same model of skin infection that we used to obtain our proteomic results and monitored the size of the lesion formed. On day five of the infection, we excised and homogenized each abscess and performed serial dilutions to count the number of CFUs present.

Of the mutants tested, only one demonstrated a decrease in the severity of infection compared to wild-type MRSA in both the size of the lesion formed (Fig 3.4B, Fig S3.6) and the number of CFUs within the abscess (Fig 3.4C, S3.6). This mutant with a hindered ability to infect has an insertion within the bifunctional aldehyde-alcohol dehydrogenase (AdhE) gene (SAUSA300_0151) ($\Delta adhE$). Mutants that exhibited no decrease in infection included an iron-containing alcohol dehydrogenase (Δadh), threonine dehydratase ($\Delta tdcB$), alanine dehydrogenase ($\Delta ald1$), SAUSA300_2375, SAUSA300_2132, sialic acid lyase ($\Delta nanA$), pseudouridine synthase ($\Delta psuG$), and SAUSA300_1393. Notably, deletion of the AdhE protein decreases the pathogen's virulence to a more significant degree than the $\Delta srtA$ knockout in this infection model.

To control for possible pleiotropic effects of the insertion, we re-inserted *adhE* into the chromosome under its endogenous promoter using an engineered *attB2* integrase site that does not disrupt any known genes to generate $\Delta adhE/adhE^+$ (31). The virulence of the $\Delta adhE$ mutant was restored in both lesion size (Fig 3.4D), and number of CFUs recovered (Fig 3.4E) by this complementation strain, suggesting that indeed, this protein was contributing to virulence.

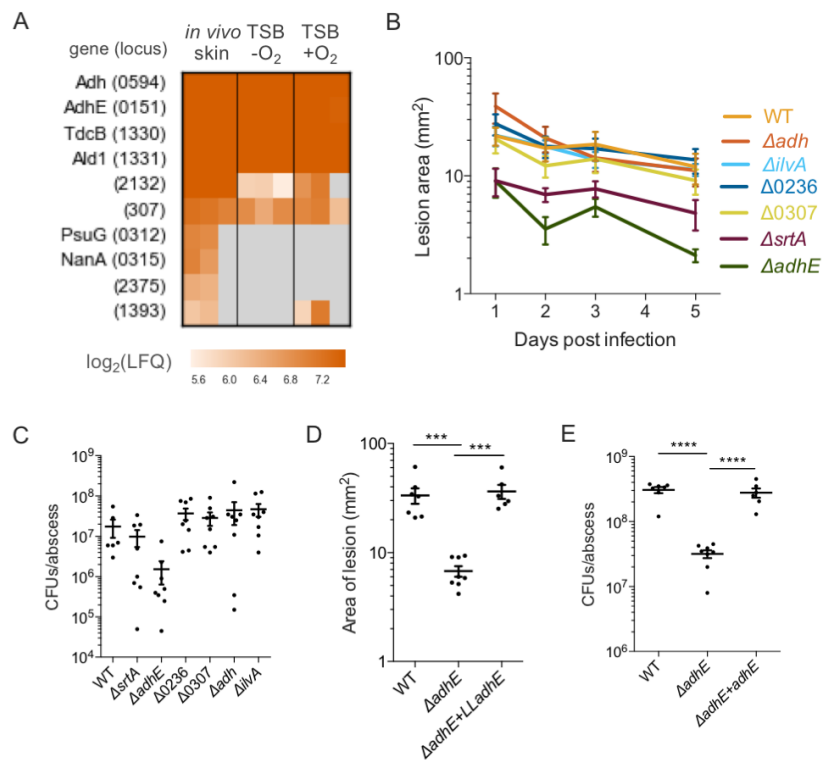


Figure 3.4: Screening of mutant hits from BONCAT analysis reveals AdhE as a novel proteomic factor important for MRSA infection. A) Proteins found during skin infection chosen to test for contributions to virulence. B) Quantification of lesion areas formed over five days after subcutaneous (S/C) injection with 2e6 CFUs of wild-type (WT) USA300 strain JE2 or selected transposon mutants found in BONCAT screen. C) CFUs recovered from abscess in 3.5B. D) Quantification of lesion areas formed with complemented strain of AdhE on day two of skin infection. E) CFUs recovered from abscess in 3.5D.

The $\Delta adhE$ mutant shows no phenotype *in vitro*. AdhE is an 869-amino acid-long protein important for fermentative growth under redox stress (32) (Fig 3.5A). We found AdhE to be significantly upregulated during anaerobic growth and *in vivo* compared to aerobic conditions. Additionally, it was one of the top proteins that PCA revealed contributed to differences in expression profiles between *in vitro* and *in vivo* samples (Fig S3.16). Although AdhE has not been studied in great detail with respect to *S. aureus*, studies of its homologs in other bacteria such as *E. coli* may afford clues towards its function *in vivo*. AdhE is important for adhesion and peroxide resistance in *E. coli* (33, 34), adhesion in *Listeria monocytogenes* (35), and virulence in *Streptococcus pneumoniae* (36).

However, *S. aureus* $\Delta adhE$ strains showed no defect in hemolysis, pigment formation, or mannitol fermentation (37). Notably, the $\Delta adhE$ knockout grew the same as wild-type *S. aureus* on all carbon sources tested, including during aerobic and anaerobic growth (Fig S7A), did not change its growth rate in response to peroxide (Fig S3.7B), and did not appear to affect its ability to adhere to cells in culture (Fig S3.7C). This lack of phenotype highlights the inability of *in vitro* models of infection to accurately reflect the phenotype *in vivo* and validates the method of proteomic analysis during infection *in vivo* rather than during infection *in vitro*.

A single point mutation in AdhE decreases *S. aureus* infection. We sought to determine whether the catalytic activity of the AdhE protein contributed to infection. In

Entamoeba histolytica, the alcohol dehydrogenase activity of the C-terminal domain was dependent on the presence of an active N-terminal aldehyde dehydrogenase domain (38). We mutated the cysteine homologous to the reported catalytic cysteine within the aldehyde dehydrogenase domain to an alanine residue (C258A, Fig 3.5B) and inserted this mutant into $\Delta adhE$ to see if it could recapitulate infection as well as wild-type or the AdhE complemented strain (39). The C258A mutation reduced the levels of infection to the levels of the $\Delta adhE$, indicating that a mutation within a single residue of AdhE is enough to decrease virulence (Fig 3.5D, 3.5E, S3.8)

Disulfiram decreases the severity of infection. Knowing that a single mutation drastically decreased the severity of MRSA skin infection, we postulated that targeting this residue could serve as a novel anti-infective strategy. The anti-alcoholism drug disulfiram (Antabuse) is reported to irreversibly carbamylate the conserved catalytic cysteine in the human homolog of the aldehyde dehydrogenase domain of AdhE, ALDH1A1 (40). Disulfiram was also shown to decrease the ability of *E. histolytica* to ferment through inhibition of its AdhE activity (38). The *E. histolytica* AdhE shares 71% positive homology with *S. aureus* AdhE so we tested if it would also decrease MRSA virulence within the skin, even though it has reported weak antibiotic activity *in vitro* (41). We also did not note differences in growth rate in the presence of disulfiram (Fig S3.13). Injection of disulfiram into mice as they were infected with MRSA led to a significant reduction in both the size of the lesion and number of CFUs recovered compared to vehicle (Fig 3.5E, 3.5F).

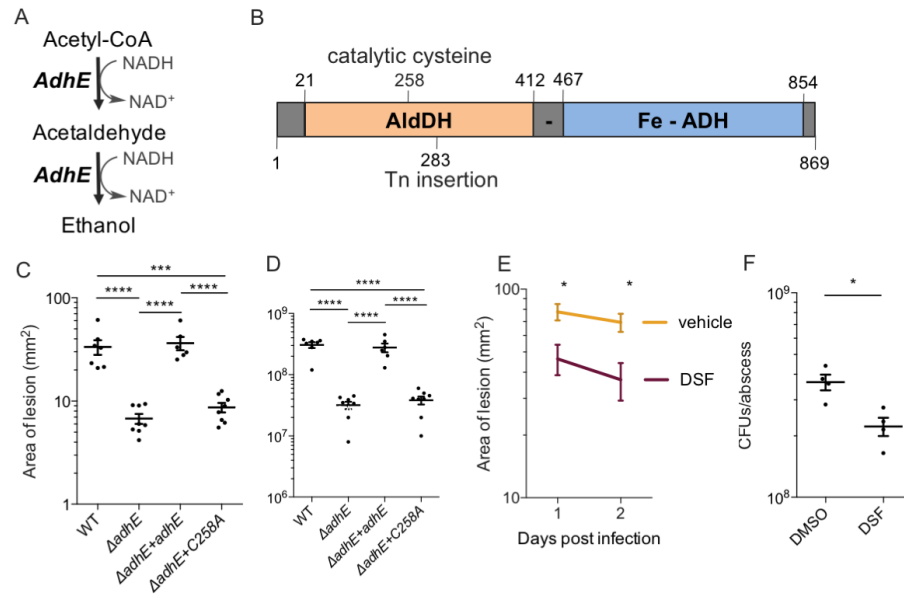


Figure 3.5: The metabolic role of AdhE during infection. A) Fermentative pathway AdhE is annotated as important during low oxygen environments. B) Cartoon representation of the bifunctional enzyme. C) Area of lesion formed during complementation with the C258A mutant compared to wild-type (WT) after two days of infection. D) CFUs / abscess obtained in experiment 3.5D. E) Area of lesion formed after DSF treatment. F) CFUs / abscess obtained in experiment 3.5E.

3.4 Discussion

Elucidation of the proteome of a pathogen during an *in vivo* infection is difficult; *in vitro* cultures that mimic the host environment are often used instead. However, these *in vitro* cultures do not sufficiently reflect the conditions within hosts and important factors may be missed. By using the cell-specific BONCAT method, we were able to label, visualize, and enrich proteins involved in pathogenesis within a mouse model of MRSA skin infection, overcoming some of the prior challenges associated with discovery-based proteomics of pathogens in a mammalian host. In addition to validating many known virulence factors, the proteomics results provide an unbiased snapshot of MRSA as it

infects.

This portrait of infecting MRSA reveals a pathogen hiding from the innate immune system while scavenging for nutrients by expressing proteins important for host cell lysis, antibody evasion, iron acquisition, and amino acid catabolism (Fig 3.3). While many of these proteins have previously been identified to be important for infection, we also identified some that had not been previously associated with contributing to infection. We postulate that many of these could be candidate anti-infective targets, but did not have the capabilities to screen every protein found.

By screening ten proteins significantly upregulated or uniquely found within the mouse compared to *in vitro* growth, we hoped to find proteins that are important for infecting MRSA, but are not indispensable for normal growth and viability. Targeted inhibitors of these proteins may impose less selection pressure for the microbe and suppress the development of antibiotic resistance. We were fortunate to find a protein, AdhE, which fit these characteristics. Disrupting AdhE does not cause defects to growth *in vitro*, which may have led to it not previously being identified as important for MRSA infection (Fig S3.11). A single point mutation to the catalytic cysteine within AdhE significantly decreased the levels of infection, which is surprising as the MRSA genome contains many redundancies (5). For example, we also found a related alcohol dehydrogenase (Adh) highly upregulated in the skin infection proteome, but when we tested an Δadh mutant *in vivo*, we saw no decrease in its ability to infect (Fig 3.4A-C).

Understanding the molecular mechanism of AdhE's contributions to infection and fermentation the abscess will require further study. The redox sensor Rex regulates expression of AdhE, suggesting that during adaptation to early infection, *S. aureus* expresses proteins important in maintaining the redox balance of NADH/NAD⁺ (42). Previous studies have indicated that the pathogenic nature of MRSA depends on its ability to ferment within the low oxygen environment of the abscess (23, 43, 44). While L-lactate fermentation is critical for renal infection, especially during nitrosative stress (45), fermenting MRSA have also been shown to produce ethanol and formate (41). Supporting this theory, a study of a *S. aureus* infection in a human prosthetic joint detected the presence of both lactate and ethanol in the joint fluid (46). While disulfiram significantly minimized the infection, the drug also inhibits the mammalian ALDH1A1. We postulate that more specific therapies related to disulfiram's structure could be created to target the C258 residue in *S. aureus* in particular with higher specificity and affinity. Overall, targeting AdhE and pathogenic fermentation in general has therapeutic potential as it augments the innate immune system and decreases infection severity.

Finally, we hypothesize that application of this approach to other pathogens and animal models of infection would be straightforward and could yield important insights into both the dynamic environment that pathogens see during infection and their subsequent response to these fluctuations. We envision that by placing the NLL-MetRS under different promoters cell- and state-selective BONCAT may be achieved to label

additional subpopulations within infections.

3.5 Materials & Methods

Ethics statement. Animal experiments were performed in accordance with the regulations for the Institutional Animal Care and Use Committee at Caltech. The investigators were not blinded to the experimental conditions.

Culture conditions. Bacteria were grown at 37 °C in LB (*E. coli*), or tryptic soy (*S. aureus*) medium or on agar plates supplemented with 100 µg/mL ampicillin, 10 µg/mL erythromycin, 50 µg/mL spectinomycin, 10 µg/mL chloramphenicol (RN4220), 20 µg/mL chloramphenicol (USA300), or 5 µg/mL tetracycline as needed. Azidonorleucine hydrochloride (Iris Biotech) was dissolved in PBS and brought to a pH of 7.5 using 1 M NaOH for a final concentration of 100 mM. This stock solution was diluted in PBS for all subsequent labeling studies.

Bacterial strains and plasmids. A complete list of the strains and primers used can be found in Supplementary Tables 1 and 2. *S. aureus* mutant strains were generated from the *S. aureus* clinical isolate JE2 (USA300). Wild-type strains and all isogenic mutants were provided by the Network on Antimicrobial Resistance in *Staphylococcus aureus* (NARSA) for distribution by BEI Resources, NIAID, NIH (47). Transposon insertions were verified through sequencing prior to use (47).

The *E. coli* mutant NLL methionyl-tRNA synthetase was codon-optimized for *S. aureus* (Genscript) and inserted into the backbone of pmRFPmars (a gift from Martin Fraunholz (18), Addgene plasmid # 26252) using ligation-independent cloning to remove the mRFP and insert an inducible NLL-MetRS (pSS20_tet). The tetR promoter was removed and the hprK promoter amplified from the USA300 genome was inserted in front of the NLL-MetRS using the Sall and KpnI sites to make the plasmids pSS20_hprK. These plasmids were confirmed through sequencing (Table S3.3). This plasmid was electroporated into the cloning strain of *S. aureus* RN4220 and the isolated plasmid from this strain was electroporated into strain JE2 (USA300).

Chromosomal integration of AdhE was achieved using the system created by Lei et al (31). We amplified AdhE and its endogenous promoter from the USA300 chromosome and inserted this fragment into the multiple cloning site of plasmid pLL102 to create pLL102_adhE. We inserted this plasmid by electroporation into a strain of RN4220 that has the engineered integration site and expresses the corresponding integrase (strain CYL12349). This chromosomal insertion was then transduced using Φ 85 phage into the JE2 Δ AdhE mutant strain. Using the same method, the empty pLL102 plasmid was also incorporated into wild-type JE2 and the Δ AdhE strain for controls.

BONCAT labeling in TSB. Overnight cultures of *S. aureus* (+NLL or -NLL) were diluted 100-fold into 2 mL of fresh TSB with chloramphenicol. When the cultures reached an OD of \sim 0.3, AnI was added to a final concentration of 2 mM for 1 hour. The samples

were spun down, resuspended in 200 μ L TSM (50 mM Tris, 500 mM sucrose, 10 mM MgCl_2), and lysed with 1 μ g of lysostaphin at 37 °C for 1 hour. The samples were brought to 1% SDS and the manufacturer's instructions were followed for the Click-It Kit with alkyne-TAMRA (Thermo Scientific).

Mouse infection and *in vivo* labeling studies. Skin infections were performed according to previously described methods (4). Briefly, overnight cultures of *S. aureus* were diluted 100-fold into 5 mL of fresh TSB. The culture was grown at 37 °C for 2-2.5 hours with shaking until the $\text{OD}_{600} = 0.48$. Cultures were washed with PBS and resuspended to achieve a concentration of $\sim 2 \times 10^7$ cells/ 50 μ L. For each experiment, a dilution series of every strain to be injected was plated in duplicate for an estimate of cell count injected into each animal.

8-week-old female C57BL/6J mice (Jackson Labs, #000664) housed under specific-pathogen free (SPF) conditions were shaved and treated with Nair on their flanks at least a day prior to infection. On the day of infection, mice were anesthetized with isoflurane and inoculated by subcutaneous (S/C) injection in each flank with $\sim 2 \times 10^7$ CFU in 50 μ L D-PBS. For AnI labeling experiments, 25 μ L of 50 mM AnI was injected along with *S. aureus*. Each day the lesions on the mice were measured by calipers and photographed for image processing using ImageJ. At the indicated timepoint, mice were killed by CO_2 asphyxiation, and abscesses were excised and homogenized in 1 mL of 1% Triton X-100 in PBS. Dilution series of the homogenates were plated on agar for enumeration of viable

MRSA. Statistical analysis was performed with ANOVA corrected for multiple hypothesis testing with Dunnett's method using Prism (GraphPad Software, La Jolla, CA).

Cryosectioning, DBCO-staining, immunostaining, and imaging. Abscesses were excised, placed in optimum cutting temperature (O.C.T.) compound, and frozen at -80 °C. They were then cut into ~15 µm sections and deposited onto glass slides. The slides were fixed with 2% paraformaldehyde (PFA), permeabilized with 0.1% Triton-X, and treated with lysostaphin at 37 °C. The samples were next blocked in 100 mM iodoacetamide for 30 min in the dark, then reacted with 5 µM DBCO-AlexaFluor488 (Click Chemistry Tools) for 15 min. After washing, the samples were blocked with 1% mouse serum, then treated with a 1:3000 dilution of anti-*Staphylococcus aureus* antibody (polyclonal, rabbit) (Ab37644, Abcam). A goat anti-rabbit secondary antibody conjugated to AlexaFluor555 (Thermo Scientific) was then added at 1:10,000 dilution. Samples were washed with PBS, and Vectashield with DAPI was added prior to coverslips. Imaging was performed using a Zeiss LSM 880 confocal microscope with a Plan-Apochromat 10/0.45-numerical aperture M27 objective (working distance [wd], 2.0 mm). Image reconstruction and analysis was performed in the FIJI distribution of ImageJ (48).

Enrichment of azide-labeled proteins.

Proteins were enriched in parallel from +NLL or -NLL infected samples to account for nonspecific binding to beads. Homogenized abscesses in PBS were brought to 1.5% SDS and boiled. Insoluble proteins were removed and the clarified lysate was reduced for 10 min in 10 mM dithiothreitol (DTT), followed by incubation with 100 mM iodoacetamide

for 45 min in the dark to block any reactive thiols. One volume equivalent of 8 M urea was added, followed by 30 μ L of washed DBCO-agarose, and the samples were rotated end over end in the dark for 16-24 hours. Unbound proteins were washed from the agarose resin in gravity columns using 1% SDS (10 x 5 mL), 8 M urea (10 x 5 mL), and 20% acetonitrile (10 x 5 mL). An on-bead digest was performed by adding 100 ng trypsin in 10% acetonitrile (ACN) in 100 mM ammonium bicarbonate buffer. Released peptides were dried and desalted using C18 StageTips as previously described (49).

LC-MS/MS analysis. All LC-MS/MS experiments were performed on an EASY-nLC1000 coupled to a hybrid LTQ-Orbitrap Elite mass spectrometer with a nano-electrospray ion source (Thermo Fisher Scientific). Peptides were re-suspended in 0.1% (v/v) formic acid and loaded on a 15-cm reversed phase analytical column (75 μ m internal performance diameter, ID) packed in-house with 3 μ m C18AQ beads (ReproSil-Pur C18AQ, Dr. Maisch-GmbH). For LC, solvent A consisted of 97.8% H₂O, 2% ACN, and 0.2% formic acid and solvent B consisted of 19.8% H₂O, 80% ACN, and 0.2% formic acid. The samples were run on a 120 minute elution gradient from 0% (100% solvent A) to 30% Solvent B (70% solvent A) at a flow rate of 350 nL/minute. The mass spectrometer was operated in data-dependent mode to switch automatically between MS and MS/MS scans (50). Survey full scan mass spectra were acquired in the Orbitrap (400–1600 m/z) with a resolution of 60,000 at 400 m/z. The top twenty most intense ions from the survey scan were isolated and fragmented in the linear ion trap by collisionally induced dissociation (CID). Precursor ion charge state screening was enabled, and all

singly charged and unassigned charge states were rejected. The dynamic exclusion list was set with a maximum retention time of 90 seconds and a relative mass window of 10 ppm.

MS data analysis. Raw files were searched using MaxQuant(51) against the *S. aureus* strain USA300 UniProt entry (2,607 sequences), *Mus musculus* C57BL/6J UniProt entry (51,544 sequences), and an in-house contaminant database (259 sequences). The digestion enzyme was specified as trypsin with up to three missed cleavages. Carbamidomethylation of cysteine was set as a fixed modification, and protein N-terminal acetylation, N-terminal formylation, and methionine oxidation were variable modifications. We also included variable modifications of methionine corresponding to AnI or reduced AnI.

Statistical data analysis. Skin infection data was analyzed and plotted using Prism (GraphPad). All data are expressed as mean \pm SEM. Differential protein expression analysis was performed with the Bioconductor package LIMMA 3.14.1. Proteins with a corresponding fold-change P value (adjusted for multiple hypothesis testing with the Benjamini-Hochberg method) lower than 0.05 were accepted as differentially expressed.

Disulfiram testing. Mice were gavaged with 160 mg/kg disulfiram (Pharmaceutical grade, Sigma) or vehicle the day before and the day of infection.

Supporting Information. For details regarding experimental methods and supplementary figures, see Supporting Materials and Methods (Appendix A).

References

1. Thurlow LR, Joshi GS, & Richardson AR (2012) Virulence strategies of the dominant USA300 lineage of community-associated methicillin-resistant *Staphylococcus aureus* (CA-MRSA). *Fems Immunol Med Mic* 65(1):5-22.
2. Thomer L, Schneewind O, & Missiakas D (2016) Pathogenesis of *Staphylococcus aureus* Bloodstream Infections. *Annu Rev Pathol-Mech* 11:343-364.
3. Wang Y, *et al.* (2017) Mouse model of hematogenous implant-related *Staphylococcus aureus* biofilm infection reveals therapeutic targets. *Proc Natl Acad Sci* 114(26):E5094-E5102.
4. Kennedy AD, *et al.* (2010) Targeting of alpha-hemolysin by active or passive immunization decreases severity of USA300 skin infection in a mouse model. *J Infect Dis* 202(7):1050-1058.
5. Diep BA, *et al.* (2014) Identifying Potential Therapeutic Targets of Methicillin-resistant *Staphylococcus aureus* Through *in Vivo* Proteomic Analysis. *J Infect Dis* 209(10):1533-1541.
6. Becker D, *et al.* (2006) Robust *Salmonella* metabolism limits possibilities for new antimicrobials. *Nature* 440(7082):303-307.
7. Otto A, van Dijl JM, Hecker M, & Becher D (2014) The *Staphylococcus aureus* proteome. *Int J Med Microbiol* 304(2):110-120.
8. Olive AJ & Sasseti CM (2016) Metabolic crosstalk between host and pathogen: sensing, adapting and competing. *Nat Rev Microbiol* 14(4):221-234.
9. Stone SE, Glenn WS, Hamblin GD, & Tirrell DA (2017) Cell-selective proteomics for biological discovery. *Curr Opin Chem Biol* 36:50-57.
10. Yuet KP, *et al.* (2015) Cell-specific proteomic analysis in *Caenorhabditis elegans*. *Proc Natl Acad Sci* 112(9):2705-2710.
11. Mahdavi A, *et al.* (2014) Identification of secreted bacterial proteins by noncanonical amino acid tagging. *Proc Natl Acad Sci* 111(1):433-438.
12. Ngo JT, Schuman EM, & Tirrell DA (2013) Mutant methionyl-tRNA synthetase from bacteria enables site-selective N-terminal labeling of proteins expressed in mammalian cells. *Proc Natl Acad Sci* 110(13):4992-4997.

13. Grammel M, Dossa PD, Taylor-Salmon E, & Hang HC (2012) Cell-selective labeling of bacterial proteomes with an orthogonal phenylalanine amino acid reporter. *Chem Commun* 48(10):1473-1474.
14. Wier GM, McGreevy EM, Brown MJ, & Boyle JP (2015) New Method for the Orthogonal Labeling and Purification of *Toxoplasma gondii* Proteins While Inside the Host Cell. *Mbio* 6(2):e01628-01614.
15. Chande AG, *et al.* (2015) Selective enrichment of mycobacterial proteins from infected host macrophages. *Sci Rep-Uk* 5:13430.
16. Ngo JT, *et al.* (2009) Cell-selective metabolic labeling of proteins. *Nat Chem Biol* 5(10):715-717.
17. Bateman BT, Donegan NP, Jarry TM, Palma M, & Cheung AL (2001) Evaluation of a tetracycline-inducible promoter in *Staphylococcus aureus* *in vitro* and *in vivo* and its application in demonstrating the role of sigB in microcolony formation. *Infect Immun* 69(12):7851-7857.
18. Paprotka K, Giese B, & Fraunholz MJ (2010) Codon-improved fluorescent proteins in investigation of *Staphylococcus aureus* host pathogen interactions. *J Microbiol Methods* 83(1):82-86.
19. Bubeck Wardenburg J, Williams WA, & Missiakas D (2006) Host defenses against *Staphylococcus aureus* infection require recognition of bacterial lipoproteins. *Proc Natl Acad Sci* 103(37):13831-13836.
20. Kammers K, Cole RN, Tiengwe C, & Ruczinski I (2015) Detecting Significant Changes in Protein Abundance. *EuPA Open Proteom* 7:11-19.
21. Ritchie ME, *et al.* (2015) limma powers differential expression analyses for RNA-sequencing and microarray studies. *Nucleic Acids Res* 43(7): e47.
22. Carneiro CRW, Postol E, Nomizo R, Reis LFL, & Brentani RR (2004) Identification of enolase as a laminin-binding protein on the surface of *Staphylococcus aureus*. *Microbes Infect* 6(6):604-608.
23. Halsey CR, *et al.* (2017) Amino Acid Catabolism in *Staphylococcus aureus* and the Function of Carbon Catabolite Repression. *Mbio* 8(1): e01434-16.
24. Yajjala VK, *et al.* (2016) Resistance to Acute Macrophage Killing Promotes Airway Fitness of Prevalent Community-Acquired *Staphylococcus aureus* Strains. *J Immunol* 196(10):4196-4203.
25. Mazmanian SK, *et al.* (2003) Passage of heme-iron across the envelope of *Staphylococcus aureus*. *Science* 299(5608):906-909.
26. Thurlow LR, *et al.* (2013) Functional Modularity of the Arginine Catabolic Mobile Element Contributes to the Success of USA300 Methicillin-Resistant *Staphylococcus aureus*. *Cell Host Microbe* 13(1):100-107.
27. Bae T, *et al.* (2004) *Staphylococcus aureus* virulence genes identified by bursa aurealis mutagenesis and nematode killing. *Proc Natl Acad Sci* 101(33):12312-12317.
28. Chatterjee SS, *et al.* (2013) Essential *Staphylococcus aureus* toxin export system. *Nat Med* 19(3):364-367.
29. Cheng AG, *et al.* (2009) Genetic requirements for *Staphylococcus aureus* abscess formation and persistence in host tissues. *Faseb J* 23(10):3393-3404.

30. Cascioferro S, Totsika M, & Schillaci D (2014) Sortase A: An ideal target for anti-virulence drug development. *Microb Pathogenesis* 77:105-112.
31. Lei MG, *et al.* (2012) A single copy integration vector that integrates at an engineered site on the *Staphylococcus aureus* chromosome. *BMC Res Notes* 5:5.
32. Fuchs S, Pane-Farre J, Kohler C, Hecker M, & Engelmann S (2007) Anaerobic gene expression in *Staphylococcus aureus*. *J Bacteriol* 189(11):4275-4289.
33. Beckham KSH, *et al.* (2014) The metabolic enzyme AdhE controls the virulence of *Escherichia coli* O157:H7. *Mol Microbiol* 93(1):199-211.
34. Echave P, Tamarit J, Cabiscol E, & Ros J (2003) Novel antioxidant role of alcohol dehydrogenase E from *Escherichia coli*. *J Biol Chem* 278(32):30193-30198.
35. Burkholder KM & Bhunia AK (2010) *Listeria monocytogenes* Uses Listeria Adhesion Protein (LAP) To Promote Bacterial Transepithelial Translocation and Induces Expression of LAP Receptor Hsp60. *Infect Immun* 78(12):5062-5073.
36. Luong TT, *et al.* (2015) Ethanol-Induced Alcohol Dehydrogenase E (AdhE) Potentiates Pneumolysin in *Streptococcus pneumoniae*. *Infect Immun* 83(1):108-119.
37. Lorenz N, Clow F, Radcliff FJ, & Fraser JD (2013) Full functional activity of SSL7 requires binding of both complement C5 and IgA. *Immunol Cell Biol* 91(7):469-476.
38. Espinosa A, *et al.* (2001) The bifunctional *Entamoeba histolytica* alcohol dehydrogenase 2 (EhADH2) protein is necessary for amebic growth and survival and requires an intact C-terminal domain for both alcohol dehydrogenase and acetaldehyde dehydrogenase activity. *J Biol Chem* 276(23):20136-20143.
39. Zheng TY, *et al.* (2015) Cofactor Specificity of the Bifunctional Alcohol and Aldehyde Dehydrogenase (AdhE) in Wild-Type and Mutant *Clostridium thermocellum* and *Thermoanaerobacterium saccharolyticum*. *J Bacteriol* 197(15):2610-2619.
40. Koppaka V, *et al.* (2012) Aldehyde Dehydrogenase Inhibitors: a Comprehensive Review of the Pharmacology, Mechanism of Action, Substrate Specificity, and Clinical Application. *Pharmacol Rev* 64(3):520-539.
41. Ejim L, *et al.* (2011) Combinations of antibiotics and nonantibiotic drugs enhance antimicrobial efficacy. *Nat Chem Biol* 7(6):348-350.
42. Pagels M, *et al.* (2010) Redox sensing by a Rex-family repressor is involved in the regulation of anaerobic gene expression in *Staphylococcus aureus*. *Mol Microbiol* 76(5):1142-1161.
43. Park MK, Myers RAM, & Marzella L (1992) Oxygen-Tensions and Infections - Modulation of Microbial-Growth, Activity of Antimicrobial Agents, and Immunological Responses. *Clin Infect Dis* 14(3):720-740.
44. Vitko NP, Spahich NA, & Richardson AR (2015) Glycolytic Dependency of High-Level Nitric Oxide Resistance and Virulence in *Staphylococcus aureus*. *Mbio* 6(2): e00045-15.

45. Spahich NA, Vitko NP, Thurlow LR, Temple B, & Richardson AR (2016) *Staphylococcus aureus* lactate- and malate-quinone oxidoreductases contribute to nitric oxide resistance and virulence. *Mol Microbiol* 100(5):759-773.
46. Xu YJ, *et al.* (2016) *In vivo* gene expression in a *Staphylococcus aureus* prosthetic joint infection characterized by RNA sequencing and metabolomics: a pilot study. *BMC Microbiol* 16:80.
47. Fey PD, *et al.* (2013) A Genetic Resource for Rapid and Comprehensive Phenotype Screening of Nonessential *Staphylococcus aureus* Genes. *Mbio* 4(1).
48. Schindelin J, *et al.* (2012) Fiji: an open-source platform for biological-image analysis. *Nat Methods* 9(7):676-682.
49. Rappsilber J, Mann M, & Ishihama Y (2007) Protocol for micro-purification, enrichment, pre-fractionation and storage of peptides for proteomics using StageTips. *Nat Protoc* 2(8):1896-1906.
50. Kalli A & Hess S (2012) Effect of mass spectrometric parameters on peptide and protein identification rates for shotgun proteomic experiments on an LTQ-orbitrap mass analyzer. *Proteomics* 12(1):21-31.
51. Cox J & Mann M (2008) MaxQuant enables high peptide identification rates, individualized p.p.b.-range mass accuracies and proteome-wide protein quantification. *Nat Biotechnol* 26(12):1367-1372.